4666–4680 *Nucleic Acids Research, 2012, Vol. 40, No. 10* *Published online 31 January 2012*
doi:10.1093/nar/gks013

Fidelity of tRNA 5′-maturation: a possible basis for the functional dependence of archaeal and eukaryal RNase P on multiple protein cofactors

Wen-Yi Chen[1,2,3], Deepali Singh[1,3], Lien B. Lai[1,3], Michael A. Stiffler[1,3], Hue D. Lai[1,3], Mark P. Foster[1,3] and Venkat Gopalan[1,2,3,*]

[1]Department of Biochemistry, [2]Molecular, Cellular and Developmental Biology Program and [3]Center for RNA Biology, The Ohio State University, Columbus, OH 43210, USA

Received November 22, 2011; Revised December 20, 2011; Accepted December 23, 2011

ABSTRACT

RNase P, which catalyzes tRNA 5′-maturation, typically comprises a catalytic RNase P RNA (RPR) and a varying number of RNase P proteins (RPPs): 1 in bacteria, at least 4 in archaea and 9 in eukarya. The four archaeal RPPs have eukaryotic homologs and function as heterodimers (POP5•RPP30 and RPP21•RPP29). By studying the archaeal *Methanocaldococcus jannaschii* RPR's *cis* cleavage of precursor tRNA^{Gln} (pre-tRNA^{Gln}), which lacks certain consensus structures/sequences needed for substrate recognition, we demonstrate that RPP21•RPP29 and POP5•RPP30 can rescue the RPR's mis-cleavage tendency independently by 4-fold and together by 25-fold, suggesting that they operate by distinct mechanisms. This synergistic and preferential shift toward correct cleavage results from the ability of archaeal RPPs to selectively increase the RPR's apparent rate of correct cleavage by 11 140-fold, compared to only 480-fold for mis-cleavage. Moreover, POP5•RPP30, like the bacterial RPP, helps normalize the RPR's rates of cleavage of non-consensus and consensus pre-tRNAs. We also show that archaeal and eukaryal RNase P, compared to their bacterial relatives, exhibit higher fidelity of 5′-maturation of pre-tRNA^{Gln} and some of its mutant derivatives. Our results suggest that protein-rich RNase P variants might have evolved to support flexibility in substrate recognition while catalyzing efficient, high-fidelity 5′-processing.

INTRODUCTION

The biogenesis of transfer RNAs (tRNAs) involves 5′- and 3′-maturation, intron splicing (where applicable) and nucleotide modification before their use in translation (1). RNase P, the endonuclease that catalyzes the 5′-maturation, is typically a ribonucleoprotein (RNP) complex except for some organellar variants (2,3). It contains one catalytic RNase P RNA (RPR) and a varying number of RNase P proteins (RPPs): 1 in bacteria, at least 4 in archaea and 9 in eukarya (4–9). Although pre-tRNA cleavage is associated with the RPR (10–12), both RPR and RPP(s) are essential for cellular viability (13–15). While the bacterial RPP is unrelated to archaeal/eukaryal RPPs, four archaeal RPPs, which share homology with eukaryal counterparts, function as binary complexes (POP5•RPP30 and RPP21•RPP29) (16–20). The increasing protein content in the RNase P holoenzyme (10% in bacterial, 50% in archaeal and 70% in eukaryal RNase P) is accompanied by a decrease in the cleavage activity of the respective RPRs (bacterial, 10/min > archaeal, 10^{-1}/min > eukaryal, 10^{-5}/min; pH 6) (11,16,21). However, since all the holoenzymes display similar k_{cat}/K_m values (7), it is evident that archaeal and eukaryal RNase P, in contrast to their bacterial counterparts, display an acute functional dependence on multiple RPPs. We have focused on this aspect in the current investigation, particularly on how the multiple RPPs contribute to the RPR's fidelity of processing.

Given the wide variation in pre-tRNA sequences, several studies have focused on mapping the common determinants that permit the collective recognition and efficient cleavage of pre-tRNAs by RNase P. How does RNase P specifically hydrolyze the phosphodiester bond between the first nucleotide in the mature tRNA (N_{+1}) and

*To whom correspondence should be addressed. Tel: +1 614 292 1332; Fax: +1 614 292 6773; Email: gopalan.5@osu.edu
Present addresses:
Wen-Yi Chen, Department of Radiology, Stanford University, Stanford, CA 94305, USA.
Deepali Singh, School of Biotechnology, Gautam Buddha University, Greater Noida 201308, India.
Michael A. Stiffler, Department of Pharmacology, University of Texas Southwestern Medical Center, Dallas, TX 75390, USA.
Hue D. Lai, Sandia National Laboratories, Albuquerque, NM 87185, USA.

© The Author(s) 2012. Published by Oxford University Press.
This is an Open Access article distributed under the terms of the Creative Commons Attribution Non-Commercial License (http://creativecommons.org/licenses/by-nc/3.0), which permits unrestricted non-commercial use, distribution, and reproduction in any medium, provided the original work is properly cited.

Downloaded from https://academic.oup.com/nar/article-abstract/40/10/4666/2411132
by guest
on 23 July 2018

its preceding nucleotide in the 5′-leader (N_{-1}) (Figure 1)? Chemical modification interference mapping, crosslinking, nucleotide analog interference mapping and mutagenesis studies have identified a suite of interactions between pre-tRNAs and bacterial RNase P (22,23). Notably, these interactions include (i) recognition of the 5′-leader of pre-tRNAs by amino acid residues in a cleft in bacterial RPP (24–28); (ii) the base at N_{-1} (typically a U) in the pre-tRNA and the adenosine at position 248 in the RPR (A_{248}—*Escherichia coli* RPR numbering) (29–31); (iii) the T stem–loop (TSL) in the pre-tRNA and the P7–P11 region in the RPR, referred to as the TSL-binding site (TBS) (32–34); and (iv) Watson–Crick base pairing of the 3′-terminal RCC sequence of the pre-tRNA and a conserved GGU sequence in the L15 loop of RPR (23,35). A recent crystal structure of a bacterial RNase P holoenzyme-tRNA (ES) complex (36) confirms these intermolecular interactions. However, not all these contacts are required for accurate or efficient cleavage; hierarchy (if any) among them remains to be determined. In a related vein, differences between recognition of consensus (possessing the sequences/structures enumerated above) and non-consensus pre-tRNAs are also unclear.

Results from previous investigations suggest that bacterial and eukaryal RNase P employ different recognition determinants during pre-tRNA processing. First, a comparative study examining the ability of partially purified *Escherichia coli* (*Eco*) and HeLa RNase P holoenzymes to cleave deletion derivatives of *Thermus thermophilus* (*Tth*) pre-tRNA^{Gly}, a non-consensus substrate, concluded that while both enzymes are indifferent to the presence of an anticodon stem, deletion of the D stem–loop caused a 30-fold decrease in human RNase P activity but only 3-fold in *Eco* RNase P (37). That such an inference might partly be substrate identity dependent is borne out by another investigation with HeLa RNase P which reported that removal of the D stem–loop in *Eco* pre-tRNA^{Tyr} caused V_{max}/K_m to decrease by only 2-fold (38). Second, a model substrate comprising a 12-bp stem (similar to the acceptor-T-stem helical stack) capped with a terminal loop and flanked by a 5′-leader and 3′-RCCA trailer was shown to be cleaved by bacterial but not by partially purified human and frog RNase P (38–40). However, if this model substrate contains even a 1-nt bulge as a linker between the T and acceptor stems, it is recognized and cleaved by the native human and frog RNase P holoenzymes (38,39). A subsequent study showed that the human RPR (without RPPs) surprisingly could cleave a similar model substrate lacking a bulge, hinting that the multiple RPPs in the holoenzyme RNP complex must alter the RPR's substrate recognition (11). Third, cleavage of pre-tRNA^{His} by bacterial RNase P generates an 8-bp acceptor stem while maturation by eukaryotic RNase P yields a 7-bp acceptor stem (29,41,42). Finally, in contrast to the bacterial holoenzyme, partially purified *Schizosaccharomyces pombe* RNase P catalyzed correct cleavage of various derivatives of a non-consensus pre-tRNA (*S. pombe* pre-tRNA^{Ser} with G_{-1}) that differed in 5′- and 3′-flanking sequences (43).

The abovementioned observations motivate studies to uncover the molecular basis for parallels and differences in substrate recognition by RNase P from the three domains of life. In this study, we have focused particularly on the roles of the multiple archaeal/eukaryal RPPs in the fidelity of processing of non-consensus pre-tRNAs. Bacterial RNase P processes precursors to 4.5S RNA and tmRNA, select viral RNAs, C4 antisense RNA from bacteriophage P1 and P7, and some mRNAs, not all of which have a tRNA-like motif (44–49). Recently, human and yeast RNase P have been implicated in processing certain short-lived non-coding (nc) RNAs and mRNAs, and shown to even cleave single-stranded (ss) RNAs (50–56); intriguingly, common recognition determinants (tRNA-like or otherwise) in these substrates are not apparent. While the biological significance of processing these non-tRNA substrates by human/yeast RNase P remains to be uncovered, these findings reveal an unexpected expansion in the repertoire of substrates of eukaryotic RNase P and provide a possible basis for the association of the eukaryotic (and archaeal) RPR with multiple RPPs.

Here, we provide the first evidence that archaeal RPPs engender progressive and synergistic changes in shifting the cognate RPR's preference toward correct cleavage *in vitro* of pre-tRNA^{Gln}, a non-consensus substrate. By comparing the processing of pre-tRNA^{Gln} and several of its mutant derivatives, we also found that *in vitro* reconstituted archaeal and native archaeal/eukaryal RNase P exhibit both a higher fidelity in cleavage-site selection and a greater tolerance of structural deviations from the pre-tRNA consensus. We discuss the implications of these findings for the evolution of RNase P, especially the versatility and plasticity gains that might have resulted from association with multiple protein cofactors.

MATERIALS AND METHODS

Construction of pre-tRNA^{Gln}-AAU-*Mja* RPR

The cloning of pBT7-pre-tRNA^{Gln}-AAU-*Mja* RPR was carried out in two steps. First, two fragments, one encoding the *Synechocystis* pre-tRNA^{Gln} and the other encoding *Methanocaldococcus jannaschii* (*Mja*) RPR, were obtained separately by PCR using primer pairs pGln-S_3-M GF + pGln-S_3-M GR and pGln-S_3-M MF + pGln-S_3-M MR, respectively (Supplementary Table S1); the plasmids pT7-Gln (57) and pBT7-pre-tRNA^{Tyr}-UAU-*Mja* RPR (19) served as the corresponding templates. These two PCR products, each with a 19-nt overlap, were annealed and extended, and the extended product digested with BamHI and ligated to StuI- and BamHI-digested pBT7 (58) to obtain pBT7-pre-tRNA^{Gln}-UAU-*Mja* RPR. Second, to change the linker sequence from 5′-UAU-3′ to 5′-AAU-3′, we employed PCR-based mutagenesis. We designed primers ptGln-AAU-M F and ptGln-linker-M R (Supplementary Table S1) to flank the linker nucleotides and having 5′ extensions to replace the linker sequence. The primers are oriented outward to ensure amplification of the entire pBT7-pre-tRNA^{Gln}-UAU-*Mja* RPR plasmid with the new linker

Downloaded from https://academic.oup.com/nar/article-abstract/40/10/4666/2411132
by guest
on 23 July 2018

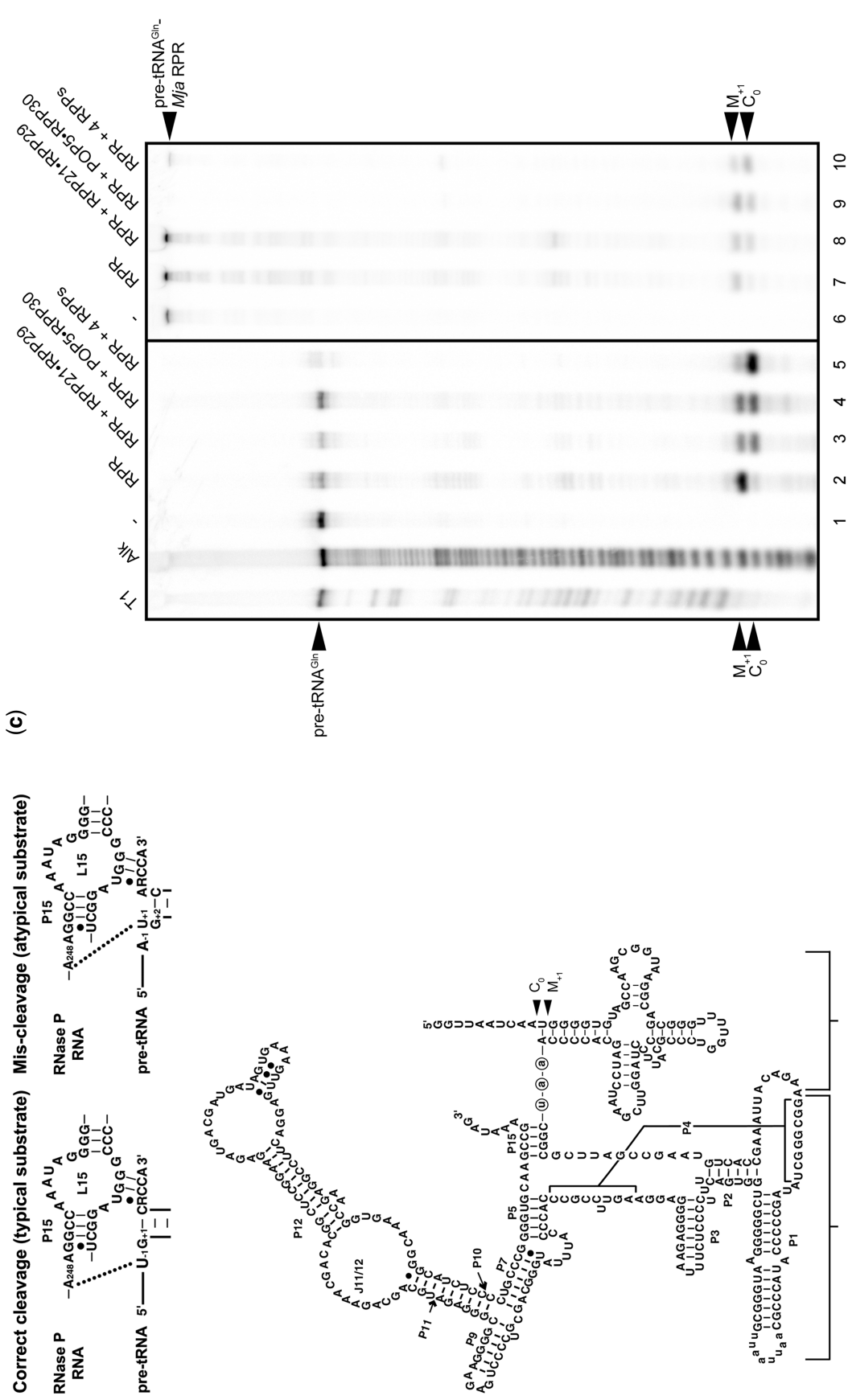

Figure 1. Archaeal RPPs affect the RPR's fidelity of processing of a non-consensus substrate. (**a**) Possible interactions around the cleavage site between nucleotides in typical (consensus) or atypical (non-consensus) pre-tRNAs and the bacterial RPR. (**b**) Secondary structure of the self-cleaving pre-tRNA^{Gln}-*Mja* RPR used in this study. The site of tethering of pre-tRNA^{Gln} to *Mja* RPR is depicted. The 5′-aau-3′ spacer is shown in circled lowercase letters. The secondary structure follows conventional representations for all RPRs (100). (**c**) Rescue of RPR's mis-cleavage by the RPPs. T1, the G ladder generated by RNase T1 digestion of pre-tRNA^{Gln}. Alk, the ladder obtained from alkaline hydrolysis of pre-tRNA^{Gln}. Uncleaved pre-tRNA^{Gln} is shown in lane 1. Cleavage of pre-tRNA^{Gln} by *Pfu* RPR, RPR + RPP21•RPP29, RPR + POP5•RPP30 and RPR + both RPP complexes is shown in lanes 2–5, respectively. Lanes 6 and 7 represent uncleaved and self-cleaved pre-tRNA^{Gln}-*Mja* RPR, respectively. The cleaved 5′-leader products generated by addition of *Mja* RPP21•RPP29, POP5•RPP30 and four RPPs to pre-tRNA^{Gln}-*Mja* RPR are shown in lanes 8–10. M_{+1}, the 5′-leader generated from mis-cleavage between positions +1 and +2 in pre-tRNA^{Gln}; C_0, the 5′-leader from cleavage at the correct site between positions −1 and +1 in pre-tRNA^{Gln}.

Downloaded from https://academic.oup.com/nar/article-abstract/40/10/4666/2411132
by guest
on 23 July 2018

sequence. The resulting PCR product was circularized by ligation with T4 DNA ligase and transformed into *Eco* DH5α. Transformants were then screened to identify those harboring the desired mutation, which were subsequently confirmed by DNA sequencing.

Construction of mutant derivatives of *Synechocystis* sp. PCC6803 pre-tRNA^{Gln}

The genes encoding various mutant derivatives of *Synechocystis* pre-tRNA^{Gln} (Figure 3) were cloned using a PCR-based strategy. The entire coding sequence was generated either from fill-in of an annealed pair of primers (Supplementary Table S2) designed to have an overlapping complement or through PCR-based mutagenesis with pT7-Gln (57) serving as the template. In some cases (where cloning into pUC19 was involved), the forward primer included the T7 RNA polymerase promoter sequence and a BamHI site, while in others the forward primer was designed for cloning as a blunt-ended fragment into StuI-digested pBT7 (58). In all cases, the reverse primer included either a HindIII or an EcoRI site for subcloning and a BstNI site for linearizing the template for subsequent run-off transcription. All cloned sequences were confirmed by DNA sequencing before further use.

In vitro transcription of RNAs used in this study

All RNAs used in this study were generated by T7 RNA polymerase-mediated run-off transcription. In the case of pre-tRNA^{Gln} and its derivatives, appropriate plasmid DNAs digested with BstNI served as the template. *Eco* and *Pyrococcus furiosus* (*Pfu*) RPRs were generated from FokI-digested pJA2′ and EcoRI-digested pBT7-PfuRPR, respectively (20,59). For the self-cleaving pre-tRNA^{Gln}-AAU-*Mja* RPR, the template for transcription was generated by PCR using the high-fidelity Phusion DNA polymerase (New England Biolabs) with pBT7-pre-tRNA^{Gln}-AAU-*Mja* RPR as the template, and 5′-TAATACGACTCACTATAGGTTAATCAATGGGG TGTAG-3′ (forward) and 5′-CTATTTCGGCTTGCACC CC-3′ (reverse) as primers. Note that the forward primer includes the T7 RNA polymerase promoter (underlined sequence). These RNAs were subjected to extensive dialysis to remove unincorporated nucleotide triphosphates and their concentrations determined based on the absorbance at 260 nm and respective extinction coefficient.

To obtain radiolabeled RNAs, the appropriate transcripts were either 5′-labeled with [γ-^{32}P]-ATP and T4 polynucleotide kinase or internally labeled by including [α-^{32}P]-ATP in the *in vitro* transcription reaction. All labeled transcripts were then gel-purified using denaturing gel electrophoresis.

Purification of bacterial and archaeal RPPs

Recombinant versions of *Eco*, *Mja* and *Pfu* RPPs were obtained after overexpression in *Eco* and subsequent purification as described previously (16,20,59,60).

Partial purification of *Arabidopsis thaliana* (*Ath*) nuclear RNase P

Arabidopsis cultured suspension cells were grown at room temperature under continuous fluorescent white light (60 μmol/m^2/s) in Gamborg B5 medium (Caisson Laboratories, Inc.) supplemented with 1.1 mg/l 2,4-dichlorophenoxy acetic acid and 0.5 g/l 2-(*N*-morpholino)ethanesulfonic acid. Seven-day-old cells were harvested by filtering through two layers of Miracloth and immediately stored at −80°C until subsequent use to prepare a whole cell extract. Ion-exchange chromatography of a clarified crude lysate using sequential SP-, DEAE- and Q-Sepharose (GE Healthcare) yielded a 400-fold purified native, nuclear RNase P. Active fractions at each step were identified with pre-tRNA processing assays using tobacco chloroplast pre-tRNA^{Gly} as the substrate. A detailed protocol will be published elsewhere (Lai, L. B. and Gopalan, V., manuscript in preparation).

RNase P assays

General. Pre-tRNA cleavage assays were performed in a thermal cycler and the reactions terminated using one assay-volume of stop dye [10 M urea, 1 mM EDTA, 0.05% (w/v) xylene cyanol, 0.05% (w/v) bromophenol blue, 20% (v/v) phenol]. The reaction products were then subjected to denaturing PAGE using either 10% or 20% (w/v) polyacrylamide/7 M urea gel electrophoresis, respectively, depending on whether the resolving length was 40 cm (e.g. Figures 1 and 4) or 18 cm (for the kinetic data shown in Figure 2).

Reconstitution of bacterial and archaeal RNase P. While *Eco* RNase P was reconstituted using 15 nM RPR and 150 nM RPP, *Pfu* and *Mja* RNase P were assembled from 20 to 40 nM RPR and a 5- or 10-fold excess amount of recombinant RPP21•RPP29 + POP5•RPP30. The buffers and methods employed for assembly are described in detail elsewhere (16,20,59,60). For the self-cleavage reactions with pre-tRNA^{Gln}-*Mja* RPR, we followed the procedure described previously for pre-tRNA^{Tyr}-*Mja* RPR (19,61); typically, it involved assembling 50 nM of the self-cleaving construct and 500 nM of the RPPs.

Cleavage assays. To compare the *trans* cleavage of pre-tRNA^{Gln} by *Pfu* RNase P with the *cis* cleavage that occurs during processing of pre-tRNA^{Gln}-*Mja* RPR (Figure 1c), we employed single-turnover assays with *Pfu* RNase P. Two 2 nM of 5′-labeled pre-tRNA^{Gln} was incubated at 55°C with either 15 μM *Pfu* RPR alone or 200 nM *Pfu* RPR reconstituted with 2 μM RPPs (Figure 1c, lanes 1–5). The times of incubation were 9 h for the reactions with *Pfu* RPR and *Pfu* RPR + RPP21•RPP29, 30 min for *Pfu* RPR + POP5•RPP30 and 10 min for *Pfu* RPR + 4 RPPs.

For calculating the rate of self-cleavage of pre-tRNA^{Gln}-*Mja* RPR with and without RPPs, we largely followed the experimental approach outlined in Chen *et al.* (61) for pre-tRNA^{Tyr}-*Mja* RPR. Some modifications were necessary to ensure robust cleavage and to reduce aggregation-related problems. Through empirical testing,

Downloaded from https://academic.oup.com/nar/article-abstract/40/10/4666/2411132
by guest
on 23 July 2018

we arrived at the optimal conditions suitable for a biphasic set-up: a pre-incubation that permits RPR assembly with RPPs while minimizing self-processing, and a cleavage reaction that is initiated by switching to conditions that engender maximal activity. The conditions for self-cleavage of pre-tRNA^{Tyr}-*Mja* RPR with and without POP5•RPP30 were the same as in Chen *et al.* (60). While the first assembly phase of pre-tRNA^{Gln}-*Mja* RPR + RPP21•RPP29 was unchanged from Chen *et al.* (61) the cleavage reaction was performed in 200 mM instead of 100 mM $Mg(OAc)_2$. For the reaction with all four RPPs, both phases were performed in 50 mM MES, pH 6 instead of pH 5.4, and the assembly was carried out in 25 mM $Ca(OAc)_2$ instead of 1 mM $Mg(OAc)_2$.

To assess the extent of mis-cleavage of pre-tRNA^{Gln} and its mutant derivatives, we performed assays under multiple-turnover conditions (Figure 4). Either a reconstituted (*Eco*, *Pfu* and *Mja*) or a partially purified native (*Ath*) RNase P variant was added to 500 nM pre-tRNA^{Gln} (wild-type or a mutant derivative), a trace amount of which was internally labeled. Incubations were performed at 37°C for *Eco*/*Ath* RNase P and 55°C for *Mja*/*Pfu* RNase P. We chose incubation periods that allowed nearly two-thirds cleavage of the substrate since our goal was to ascertain the amount of correctly and aberrantly cleaved products (and not their initial velocities of formation). The assay reactions contained 10 mM HEPES (pH 7.5 at 23°C), 10 mM $Mg(OAc)_2$, 400 mM $NH_4(OAc)$ and 5%(v/v) glycerol for *Eco* RNase P; 50 mM Tris–HCl (pH 8 at 23°C), 30 mM $MgCl_2$, 800 mM $NH_4(OAc)$ for *Pfu* and *Mja* RNase P; and 20 mM Tris–HCl (pH 8 at 23°C), 5 mM $MgCl_2$ for *Ath* RNase P.

Data analysis. The RNase P reaction contents separated by denaturing PAGE were visualized by phosphorimaging (Typhoon, GE Healthcare) and quantitated with ImageQuant (GE Healthcare) to determine the amount of correctly (P_{C_0}) and aberrantly ($P_{M_{+1}}$) cleaved products. These data were then used to calculate F_{C_0} and k_{obs} for pre-tRNA^{Gln} processing; F_{C_0} is the fraction of cleavage at the correct site relative to the total cleavage [$P_{C_0}/(P_{C_0}+P_{M_{+1}})$].

According to the parallel pathways mechanism in Scheme 1, formation of both P_{C_0} and $P_{M_{+1}}$ should exhibit the same time dependence; therefore, F_{C_0} [$P_{C_0}/(P_{C_0}+P_{M_{+1}})$] should remain constant throughout the time course. Also, while $k_{obs} = k_{C_0} + k_{M_{+1}}$, the ratio of the two products reflects the overall kinetics of each path (i.e. $P_{C_0}/P_{M_{+1}} = k_{C_0}/k_{M_{+1}}$). To obtain the k_{obs} values for self-cleavage of pre-tRNA^{Gln}-*Mja* RPR in the absence and presence of RPPs, we fit either P_{C_0} or $P_{M_{+1}}$ depending on which afforded the higher signal-to-noise ratio (i.e. P_{C_0} for the reaction with four RPPs and $P_{M_{+1}}$ for the remainder, Figure 2). For example, in the RPR alone reaction, we first obtained k_{obs} by non-linear least squares fitting $[P_{M_{+1}}]_t = Amp_{M_{+1}} \times (1 - e^{-k_{obs} \bullet t})$ using Kaleidagraph software (Synergy). This k_{obs} was in turn used to obtain Amp_{C_0} via $[P_{C_0}]_t = Amp_{C_0} \times (1 - e^{-k_{obs} \bullet t})$. For each time course being studied, the $P_{C_0}/(P_{C_0}+P_{M_{+1}})$ values were individually computed at each time point and then averaged to determine the F_{C_0}. The apparent rate constants for correct (k_{C_0}) and aberrant cleavage ($k_{M_{+1}}$) were then obtained from $k_{C_0} = k_{obs} \times F_{C_0}$ and $k_{M_{+1}} = k_{obs} \times (1 - F_{C_0})$.

Three independent time courses were analyzed to obtain a measure of standard deviation for k_{obs}, k_{C_0}, k_{M+1} and F_{C_0} (Table 2); only a representative time course is shown in Figure 2. The standard errors for the best-fit values of k_{obs} did not exceed 13% (RPR alone), 14% (RPR + RPP21•RPP29), 10% (RPR + POP5•RPP30) and 17% (RPR + 4 RPPs); the correlation coefficient was always $\geq$0.98. $Amp_{M_{+1}}$ and Amp_{C_0} were used to obtain the Amp_{total} for each of the self-cleavage reactions. Note that the Amp_{total} values are ~90% for all reactions except those with RPR + 4 RPPs, where a fraction of the RPR appears to have assembled into unproductive/partial RNP complexes resulting in a one-third lower amplitude (RPR, 93 ± 7; RPR + RPP21•RPP29, 86 ± 3; RPR + POP5•RPP30, 96 ± 1; RPR + 4 RPPs, 61 ± 2).

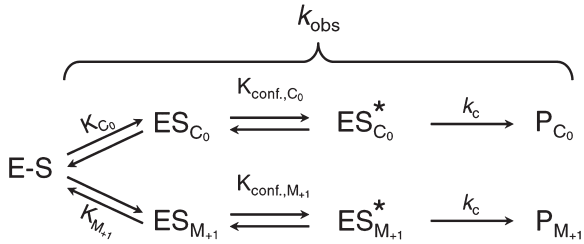

Scheme 1. E–S refers to pre-tRNA^{Gln}-*Mja* RPR with or without RPPs, and ES is the substrate-docked state.

RESULTS

Overall approach and rationale

Most bacterial pre-tRNAs possess a U_{-1} and $G_{+1}C_{+72}$ pair (62,63), and changing the N_{-1} or $N_{+1}N_{+72}$ nucleotide identity affects substrate ground-state binding, rate of pre-tRNA processing, and cleavage-site selection by bacterial RNase P (30,31,64–69). However, there are natural deviations from such a consensus and these pre-tRNAs are often mis-cleaved by bacterial RNase P, presumably due to mis-docking in the active site (Figure 1a). For example, bacterial pre-tRNA^{Gln}, which has a U_{-1} and $U_{+1}A_{+72}$, is cleaved by *Eco* RNase P correctly at C_0 (between U_{-1} and U_{+1}) and incorrectly at M_{+1} (between U_{+1} and G_{+2}) (65). Considering the interaction between U_{-1} in a typical pre-tRNA and A_{248} of the *Eco* (bacterial) RPR that is important for substrate positioning and cleavage (Figure 1a, left panel) (30), the presence of U_{+1} and G_{+2} in pre-tRNA^{Gln} probably engenders an interaction between U_{+1} in pre-tRNA^{Gln} and A_{248} in the RPR, thereby shifting the cleavage site from C_0 to M_{+1} (Figure 1a, right panel) (65). Because cleavage at M_{+1} by *Eco* RNase P occurs at only 15% to 25% frequency, the U_{+1}–A_{248} interaction is only one of several determinants that dictate the choice of cleavage site (30,32). The single bacterial RPP, which enhances the RPR's affinity for pre-tRNA/catalytically relevant Mg^{2+} and the rate of pre-tRNA cleavage (25,69–71), was reported to not

Downloaded from https://academic.oup.com/nar/article-abstract/40/10/4666/2411132
by guest
on 23 July 2018

influence the extent of mis-cleavage of pre-tRNA^{Gln} (65). Similarly, both *Eco* and *Tth* RPRs mis-cleave a human pre-tRNA^{Gly} (C_{-1}, a non-consensus substrate) with ~20% frequency regardless of the presence of their cognate RPP (37). We postulated that if the multiple archaeal (and eukaryal) RPPs provide additional substrate-recognition determinants (72) that guide the RPR's cleavage-site selection, they might engender progressive and even possibly synergistic changes in the cognate RPR's ability to cleave at the correct site of a non-consensus substrate. Prior to embarking on such an investigation, we first sought to examine the N_{-1} and N_{+1} identity variations in all tRNAs.

Although undertaken before (30), for an up-to-date analysis of the phylogenetic variation in the N_{-1} and N_{+1} identity, we examined the genomic tRNA database (62). We found that U_{-1} and G_{+1} is the predominantly favored identity in all three domains of life (Table 1), although the preference for N_{-1} is not as pronounced in Archaea and Eukarya. There are several instances when both the U_{-1} and G_{+1} substrate-recognition determinants are absent in all life forms, motivating an examination of how departure from the consensus with regard to recognition determinants is dealt with by bacterial/archaeal/eukaryal RNase P.

We chose to use a cyanobacterial pre-tRNA^{Gln} (A_{-1} and $U_{+1}A_{+72}$, Figure 1b) (57) as a reporter for our studies comparing the influence of N_{-1} and N_{+1} identity on cleavage fidelity of RNase P from all three domains of life. While there are many non-consensus variants, our choice of this pre-tRNA^{Gln} as a model was based in part on the following distribution of pre-tRNAs with A_{-1} and U_{+1}: Bacteria, 430 cases from a total of 34 782; Archaea, 1 from a total of 2497; Eukarya, 808 from a total of 37 988. Two points of note: first, the total number of archaeal tRNAs in the database is only a fraction of those reported for the bacterial/eukaryal counterparts; second, this compilation does not make assumptions on expression/function.

By exploiting our ability to assemble the archaeal RNase P holoenzyme step-wise from recombinant subunits (16–20), we quantitated the contribution of individual subsets of archaeal RPPs on cleavage-site selection and rate of processing of pre-tRNA^{Gln} by the cognate RPR. Moreover, by introducing structural alterations in pre-tRNA^{Gln}, we sought to further accentuate its mis-cleavage by bacterial RNase P and examined if such deviations from the native fold might somehow be tolerated by the archaeal and eukaryal variants.

The two archaeal RPP binary complexes differentially affect the RPR's processing fidelity and rate

We first investigated cleavage of pre-tRNA^{Gln} by *Pfu* RNase P and determined the fraction of cleavage at the correct site relative to the total cleavage: $F_{C_0} = P_{C_0}/(P_{C_0}+P_{M_{+1}})$; P_{C_0} is the product generated from cleavage at C_0 (between N_{-1} and N_{+1}) and $P_{M_{+1}}$ is that from miscleavage at M_{+1} (between N_{+1} and N_{+2}). *Pfu* RPR alone predominantly miscleaves pre-tRNA^{Gln} and exhibits an $F_{C_0} = 0.11 \pm 0.03$; with addition of either *Pfu* RPP21•RPP29 or POP5•RPP30, F_{C_0} increases to ~0.57 ± 0.03 or 0.59 ± 0.01, respectively, and further to 0.92 ± 0.01 when both complexes are present (Figure 1c, lanes 1–5). This cumulative effect of RPP21•RPP29 and POP5•RPP30 has not been reported before in any multi-protein RNase P complex. It is notable that the trend persists with some pre-tRNA^{Gln} mutant derivatives that we tested (data not shown). These results contrast with F_{C_0} being invariant during cleavage of select non-consensus pre-tRNAs by the *Eco* RPR both in the presence and absence of the RPP (37,65).

While the trans cleavage assays (under single-turnover conditions) reported above for *Pfu* RNase P provided qualitative insights on the role of RPPs, we sought to determine the apparent rates of correct and aberrant cleavage of pre-tRNA^{Gln} by an archaeal RPR with and without RPPs. By performing a titration of the enzyme over trace amounts of a consensus pre-tRNA substrate, we previously determined the maximal rate (k_{obs}) under saturating conditions of an archaeal RPR with and without RPPs (16). A similar approach with the non-consensus substrate pre-tRNA^{Gln} and *Pfu* RNase P was not possible due to the poor RPR cleavage rates at low E:S ratios and the attendant inability to accurately determine k_{obs} by fitting rate versus [*E*]. To circumvent this problem, we employed a *cis* construct that exhibits rate-limiting cleavage (19), and permits a comparison of RPR rates with and without RPPs in the context of uniform substrate binding. We appreciate that substrate interactions may have different thermodynamic or kinetic contributions in the *cis* context compared to *trans* cleavage. However, our previous studies on archaeal RNase P variants have revealed that inferences on roles of RPPs drawn from *cis* and *trans* cleavage studies mirror each other (16,19) and thereby lend merit to employment of the *cis* construct where technical advantages favor its use.

We exploited a design similar to the self-cleaving pre-tRNA^{Tyr}-S3-*Mja* RPR, which we had optimized

Table 1. Phylogenetic variation of the N_{-1} and N_{+1} identity in pre-tRNAs

Domain	Total tRNAs	Percent of tRNAs with indicated nucleotide identity							
		A_{-1}	C_{-1}	G_{-1}	U_{-1}	A_{+1}	C_{+1}	G_{+1}	U_{+1}
Bacteria	34 782	19	19	8	54	4	9	81	7
Archaea	2497	26	18	13	43	8	2	90	~0.25
Eukarya	37 988	31	17	11	41	5	2	76	16

Downloaded from https://academic.oup.com/nar/article-abstract/40/10/4666/2411132
by guest
on 23 July 2018

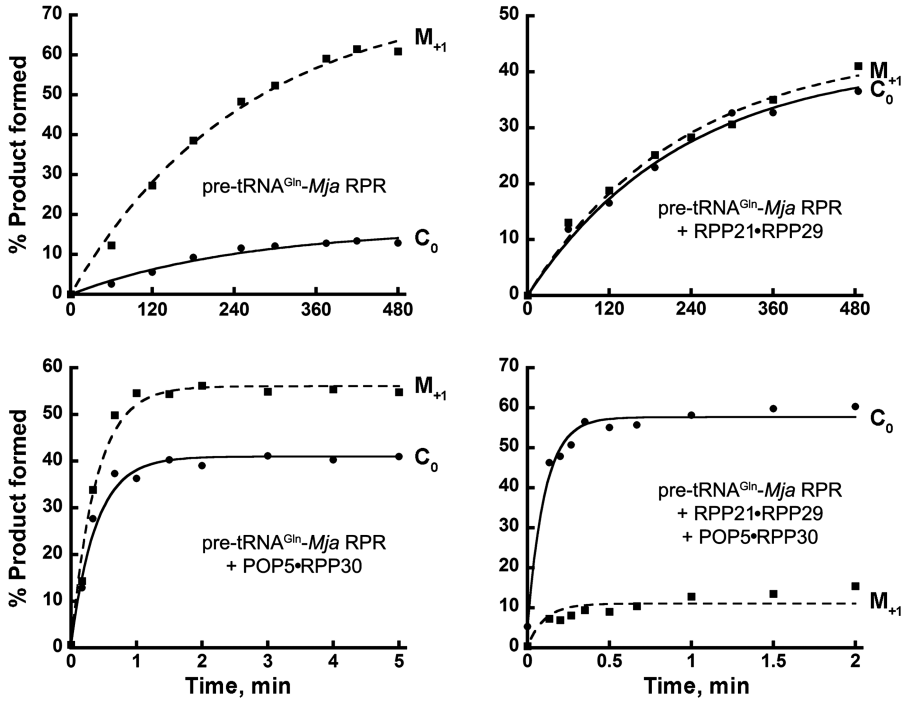

Figure 2. Effect of *Mja* RPPs on cleavage-site selection and the rate of self-cleavage of pre-tRNA^{Gln}-*Mja* RPR. Time courses depicting self-processing of pre-tRNA^{Gln}-*Mja* RPR with and without RPPs at the correct (C_0; circles) and the mis-cleaved (M_{+1}; squares) site. The mean and standard deviation values reported in Table 2 were calculated from three independent experiments, a representative of which is shown here.

earlier with regard to spacer length (3 nt, S3) and site of tethering, and whose rate-determining cleavage step we had extensively characterized both in the absence and presence of RPPs (19). For the study here, we swapped pre-tRNA^{Tyr} with pre-tRNA^{Gln} and replaced the 5′-UAU-3′ spacer in pre-tRNA^{Tyr}-S3-*Mja* RPR with a 5′-AAU-3′ spacer to obtain pre-tRNA^{Gln}-S3-*Mja* RPR. This change was introduced to prevent possible base pairing between A_{-1} and U_{+73} in the case of the original UAU spacer. For simplicity, we will refer to the new construct as pre-tRNA^{Gln}-*Mja* RPR (Figure 1b). Since the success of this strategy depends on pre-tRNA anchoring in the *cis* construct mimicking the *trans* scenario, the site of pre-tRNA tethering is critical. Our choice in pre-tRNA^{Gln}-*Mja* RPR was based on several findings on bacterial RNase P including a recent crystal structure of the RNase P holoenzyme-tRNA complex (36), which reveals base pairing of the 3′-RCC in the pre-tRNA and the L15 loop in the bacterial RPR. Therefore, we conjugated the 3′-end of pre-tRNA^{Gln} to the L15 loop-equivalent in the *Mja* RPR (Figure 1b). Control experiments described below validate this choice.

To verify that the trend observed during *cis* cleavage with *Mja* RNase P indeed parallels *trans* cleavage reactions catalyzed by *Pfu* RNase P, we examined cleavage of pre-tRNA^{Gln}-*Mja* RPR in the absence and presence of RPPs using a single time-point measurement (Figure 1c, lanes 6–10). While pre-tRNA^{Gln}-*Mja* RPR displayed $F_{C_0} = 0.14$, POP5•RPP30 and RPP21•RPP29 independently increased F_{C_0} to ~0.4 and together to ~0.8. This trend was further confirmed using time-course experiments which yielded F_{C_0} values of 0.18 ± 0.01 (−RPPs), 0.47 ± 0.02 (+RPP21•RPP29), 0.43 ± 0.01 (+POP5•RPP30), and 0.84 ± 0.03 (+ both complexes) (Table 2 and Figure 2). We also found that *Mja* RPR assembled with *Mja* RPP21•RPP29 + POP5•RPP30 displays $F_{C_0} =$ 0.8–0.9 during *trans* cleavage of pre-tRNA^{Gln} (data not shown). Collectively, these data allay concerns about an artificial bias in cleavage-site selection arising from use of the *cis*-cleaving pre-tRNA^{Gln}-*Mja* RPR in lieu of a *trans* cleavage reaction. These data also reveal that the two broad classes of euryarchaeal RNase P [type A (e.g. *Pfu*) and M (e.g. *Mja*)] (12,73) behave in a similar fashion despite the fact that only the type A RPRs support pre-tRNA cleavage in the absence of RPPs.

The time-course analyses of the self-cleavage of pre-tRNA^{Gln}-*Mja* RPR in the absence and presence of RPPs also allowed us to calculate the apparent rates of formation of correct and mis-cleaved products (k_{C_0} and $k_{M_{+1}}$). For data analysis, we employed the approach typically used to analyze first-order parallel reactions (29,31, 33,69). Here, k_{obs} for self-processing of pre-tRNA^{Gln}-*Mja* RPR is the sum of the rates of formation of P_{C_0} and $P_{M_{+1}}$. Our proposed kinetic framework (Scheme 1) for this self-cleavage parallels that for *trans* cleavage by bacterial RNase P, which was formulated based on the growing experimental evidence supporting an initial encounter complex ($E + S \leftrightarrows ES$) that undergoes a conformational change to ES* to optimally position the pre-tRNA and catalytic Mg^{2+} for efficient cleavage (74–77). During self-cleavage, the initial binding step of the *trans* reaction is replaced with a substrate-docking step ($E - S \leftrightarrows ES_{C_0}$ and $E - S \leftrightarrows ES_{M_{+1}}$, where ES_{C_0} and $ES_{M_{+1}}$ are two distinct docked states that result in different products)

Downloaded from https://academic.oup.com/nar/article-abstract/40/10/4666/2411132
by guest
on 23 July 2018

Table 2. Effect of *Mja* RPPs on the rate of cleavage and cleavage-site selection of pre-tRNA^{Gln}-*Mja* RPR at 55°C at pH 6[a]

pre-tRNA^{Gln}-*Mja* RPR	k_{obs}/min	k_{C_0}/min	$k_{M_{+1}}$/min	$k_{C_0}/k_{M_{+1}}$	F_{C_0}
Alone	0.004 ± 0.0004	0.0007 ± 0.0001	0.0031 ± 0.0003	0.2	0.18 ± 0.01
+ RPP21•RPP29	0.004 ± 0.0001	0.0021 ± 0.0001	0.0023 ± 0.0001	0.9	0.47 ± 0.02
+ POP5•RPP30	2.5 ± 0.1	1.1 ± 0.03	1.4 ± 0.07	0.8	0.43 ± 0.01
+ Both complexes	10.5 ± 0.8	7.8 ± 1.3	1.5 ± 0.5	5.2	0.84 ± 0.03

pre-tRNA^{Tyr}-*Mja* RPR	k_{obs}/min[b]
Alone	0.2 ± 0.04
+ RPP21•RPP29	0.24 ± 0.04
+ POP5•RPP30	20.5 ± 0.32
+ Both complexes	21.7 ± 0.16

pre-tRNA^{Tyr}-*Mja* RPR versus pre-tRNA^{Gln}-*Mja* RPR	$k_{obs,\text{pre-tRNA}^{Tyr}_{Gln}}/k_{C_0,\text{pre-tRNA}^{Gln}}$[c]
Alone	286
+ RPP21•RPP29	114
+ POP5•RPP30	19
+ Both complexes	2.8

[a]See 'Materials and Methods' section for a description of how k_{obs}, k_{C_0}, $k_{M_{+1}}$ and F_{C_0} were calculated. All assays were performed under optimal conditions for each catalytic entity.
[b]These data for pre-tRNA^{Tyr}–*Mja* RPR experiments are recalculated from Table 1 of reference (19). In this earlier publication, the rates reported for a self-cleaving pre-tRNA^{Tyr}–*Mja* RPR were at pH 5.4 and not pH 5.1 as was documented. To facilitate comparison of the pre-tRNA^{Gln}–*Mja* RPR and pre-tRNA^{Tyr}–*Mja* RPR cleavage experiments, the rates observed at pH 5.4 with pre-tRNA^{Tyr}–*Mja* RPR were multiplied by 4 to obtain rates that would have been observed at pH 6 should they have been manually measurable. We demonstrated previously a linear relationship between log k_{obs} and pH (19).
[c]The relative activity was obtained by dividing the k_{obs} of pre-tRNA^{Tyr}-*Mja* RPR by the apparent rate of correct cleavage (k_{C_0}) of pre-tRNA^{Gln}-*Mja* RPR.

(Scheme 1). Thus, k_{obs} cumulatively depends on the equilibrium constants for the docking steps and the rates of chemical cleavage of ES_{C_0} and $ES_{M_{+1}}$. With k_{obs} and F_{C_0} in hand, we could calculate both k_{C_0} and $k_{M_{+1}}$ (see 'Materials and Methods' section for details).

The disappearance of pre-tRNA^{Gln}-*Mja* RPR indeed followed first-order kinetics both in the absence and presence of RPPs (Figure 2). These assays were performed at pH 6 and 55°C; the lower pH helped to slow down the reaction to enable manual determination of the rates of cleavage. We summarize the key observations regarding how addition of RPPs to the RPR increased the rate and favored correct cleavage. First, there was a ~2625-fold increase in k_{obs} upon addition of the both RPP complexes to the RPR, with ~625-fold due to addition of POP5•RPP30 alone (Table 2). Second, while k_{C_0} is only one-fifth of $k_{M_{+1}}$ during self-cleavage of pre-tRNA^{Gln}-*Mja* RPR, addition of RPPs to this *cis* construct progressively and substantively increased the bias toward C_0. Although both binary RPPs independently normalize the rates of correct and mis-cleavage, their effect on k_{C_0} and $k_{M_{+1}}$ differs significantly (Table 2). RPP21•RPP29 increased k_{C_0} by 3-fold and decreased $k_{M_{+1}}$ by one-fourth, while POP5•RPP30 increased k_{C_0} and $k_{M_{+1}}$ by 1570- and 450-fold, respectively. In the presence of both complexes, k_{C_0} and $k_{M_{+1}}$ increased by 11 140- and 480-fold, respectively, reflecting a synergistic effect of the four RPPs selectively on the rate and fidelity of correct cleavage. The RPP-mediated preferential shift toward C_0 is illustrated by $k_{C_0}/k_{M_{+1}} = 0.2$ for the *cis* construct-alone reaction, 0.8–0.9 upon addition of either binary RPP, and 5.2 in the presence of four RPPs (Table 2).

Based on an in-depth study of mis-cleavage that occurred upon disrupting interactions between bacterial RNase P and the consensus nucleobase and 2′-hydroxyl at N_{-1} of the pre-tRNA, Zahler *et al.* (31) demonstrated lower affinity and cooperativity of Mg^{2+} binding for the mis-cleavage path relative to the correct cleavage. We sought to examine this possibility during cleavage of pre-tRNA^{Gln}-*Mja* RPR. Decreasing the Mg^{2+} concentration from 100 to 25 mM in the assay did not affect the F_{C_0} of pre-tRNA^{Gln}-*Mja* RPR + POP5•RPP30, but it did predictably lower the rates for both the correct and aberrant cleavage (data not shown). While it is conceivable that the F_{C_0} value might change at even lower Mg^{2+} concentrations, the weak activity at <25 mM Mg^{2+} for the RNP assembled with POP5•RPP30 precluded such experiments.

The significance of $N_{+1}N_{+72}$ for pre-tRNA cleavage-site selection decreases from bacterial > archaeal > eukaryal RNase P

Given the effect of archaeal RPPs on the RPR's processing fidelity of pre-tRNA^{Gln}, we sought to compare an RNase P holoenzyme from each domain of life with regard to cleavage-site selection of non-consensus substrates. We used *Eco*, *Pfu* and *Ath* RNase P as bacterial, archaeal and eukaryal representatives, respectively, to compare the fidelity of processing of pre-tRNA^{Gln} and its mutant derivatives (Figure 3). *Eco* and *Pfu* RNase P

Downloaded from https://academic.oup.com/nar/article-abstract/40/10/4666/2411132
by guest
on 23 July 2018

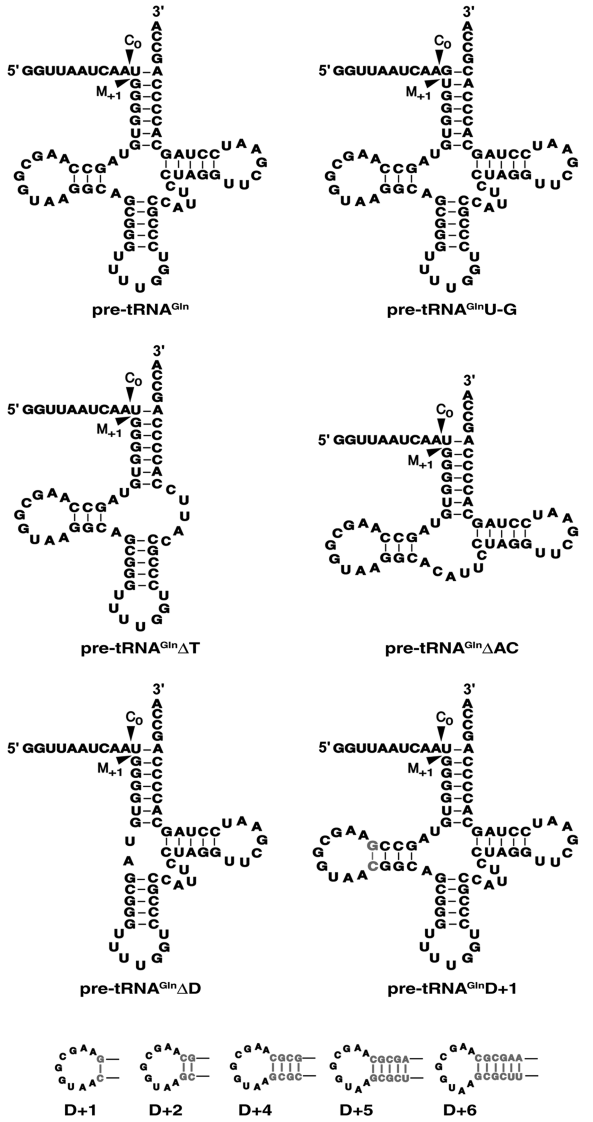

Figure 3. Schematic depicting pre-tRNA^{Gln} and its mutant derivatives used in this study.

holoenzymes were assembled *in vitro* from recombinant constituents purified using established methods (16,20,59,60). *Ath* RNase P was isolated from 7-day-old cultured suspension cells using sequential ion-exchange chromatography to yield a 400-fold purified preparation (data not shown; Lai, L. B. and Gopalan, V., unpublished results). Although studies on yeast and human nuclear RNase P show that the holoenzyme is made up of an RPR and 9 to 10 RPPs, there is still some uncertainty about the make-up of plant nuclear RNase P. Computational searches have uncovered plant homologs for a few of the known eukaryotic RPPs (78), but the identity of the plant nuclear RPR has proven elusive. Based on micrococcal nuclease and proteinase K sensitivity, however, plant nuclear RNase P (from monocots and dicots) appears to function as an RNP complex (79–81). This finding contrasts with the plant organellar version (2) whose catalytic activity is attributable to a single polypeptide [see also (82)]. For the purpose of this study, it suffices to state that the partially purified nuclear *Ath* RNase P used herein is an RNP complex likely resembling human/yeast nuclear RNase P, albeit of unknown composition.

To understand the influence of the pre-tRNA N_{-1} and N_{+1} identity on cleavage-site selection by *Eco, Pfu* and *Ath* RNase P, we studied the processing of pre-tRNA^{Gln} under multiple-turnover conditions. *Eco*, *Pfu* and *Ath* RNase P cleaved wild-type pre-tRNA^{Gln} with F_{C_0} of 0.73 ± 0.05, 0.81 ± 0.03 and 1, respectively (Figure 4). Since most pre-tRNAs contain G_{+1}, we substituted $U_{+1}A_{+72}$ in pre-tRNA^{Gln} with $G_{+1}C_{+72}$ to generate pre-tRNA^{Gln}U-G (Figure 3). While this substrate resulted in modestly higher cleavage at C_0 and a ~3-fold increase in overall cleavage rate for *Eco* RNase P (Figure 4; data not shown), some mis-cleavage remains ($F_{C_0} = 0.82 \pm 0.05$), consistent with the idea that multiple determinants dictate cleavage-site selection (30,32).

Consensus tertiary structure of pre-tRNA^{Gln} is more important for fidelity of cleavage by bacterial RNase P but not the archaeal or eukaryal variants

Upon deletion of the D-stem, increased mis-cleavage of *Tth* pre-tRNA^{Gly} by *Eco* RPR both in the presence and absence of RPP (wild-type, 3%; mutant, ~20%) was observed (37). To determine if there are differences in the relative importance of structural elements in the pre-tRNA for cleavage-site selection by the RNA- and protein-rich RNase P variants, we examined the fidelity of cleavage of three stem–loop deletion derivatives of pre-tRNA^{Gln}: ΔD, ΔAC and ΔT (Figure 3). ΔD and ΔAC were cleaved by *Eco* RNase P with F_{C_0} of 0.35 ± 0.05 and 0.15 ± 0.03, respectively, compared to 0.73 ± 0.05 observed with the wild-type (Figure 4). In contrast, *Pfu* and *Ath* RNase P cleaved ΔD and ΔAC with F_{C_0} of ~0.8 and 1, respectively, nearly identical to their cleavage of wild-type pre-tRNA^{Gln}. Interestingly, RNase P from all three domains of life failed to cleave ΔT, an observation reminiscent of previous reports on the importance of the TSL for bacterial and eukaryal RNase P recognition (37,38).

The L-shaped tertiary structure of the tRNA is dependent on the interaction between the D and TΨC loops. In fact, the importance of this interaction for tertiary structure is borne out both by the high sequence conservation of the loops and the structural compensation observed in some tRNAs to ensure preservation of the overall fold (63,83). It is therefore not unexpected that functional groups made available by the architecture of the D-TΨC loop interaction are exploited for a productive interaction with RNase P (32,33,84). As interactions between the TSL in the pre-tRNA and the TBS in the bacterial RPR do influence cleavage-site selection (32), we speculated that substrate recognition might be affected if the local TSL structure is altered, for example, by disrupting the canonical D-TΨC loop interaction. Therefore, we extended the D stem in pre-tRNA^{Gln} by 1–6 bp (D+ variants; Figure 3), and tested these mutant derivatives for correct and aberrant cleavage. Akin to the results with pre-tRNA^{Gln}ΔD, all the D+ variants were cleaved by *Eco* RNase P with F_{C_0} of 0.2–0.3 (Figure 4), while *Pfu*

Downloaded from https://academic.oup.com/nar/article-abstract/40/10/4666/2411132
by guest
on 23 July 2018

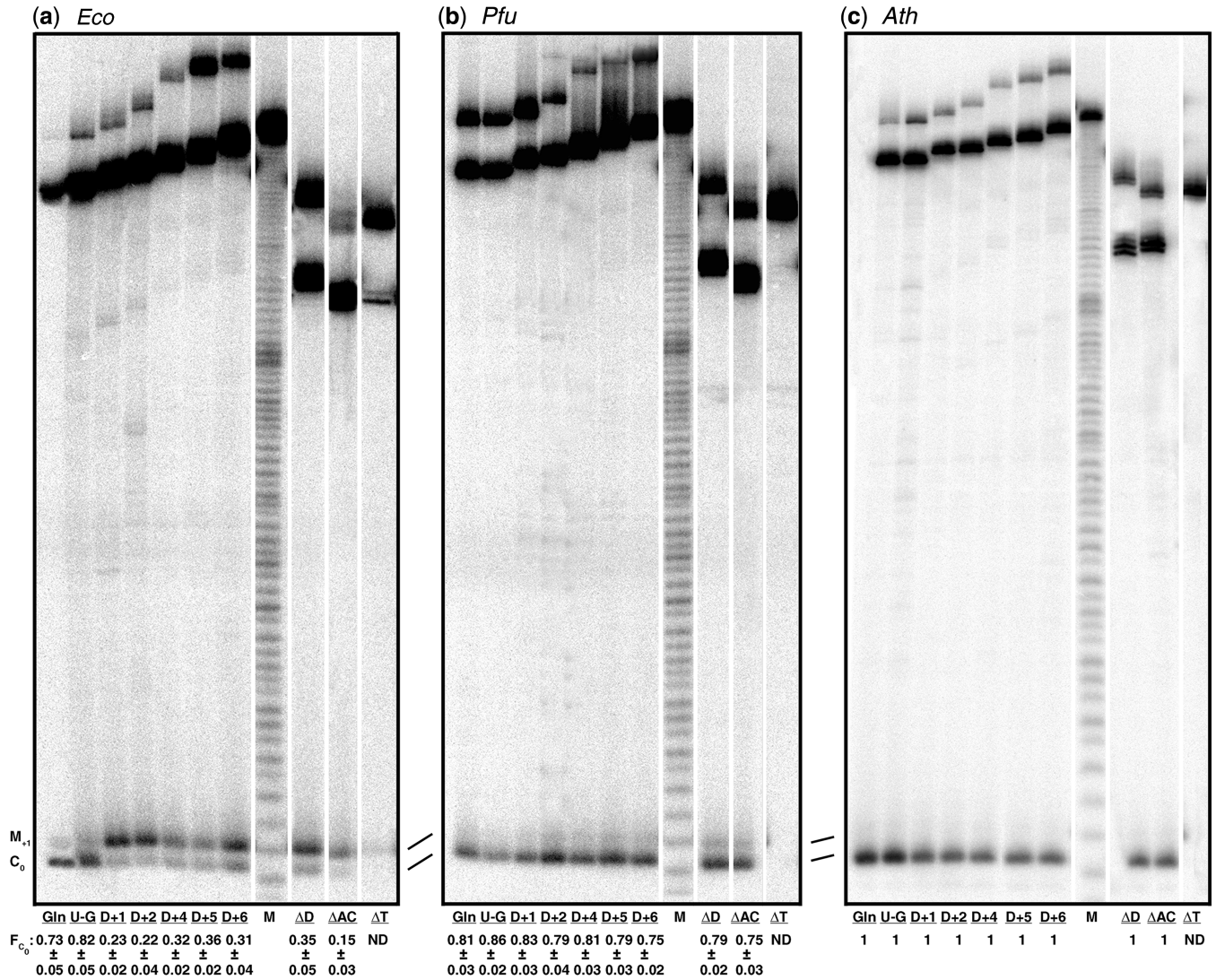

Figure 4. Comparison of correct and aberrant cleavage of pre-tRNA^{Gln} and its mutant derivatives by different RNase P holoenzymes. Representative assay gels depicting the cleavages by (**a**) *Eco*, (**b**) *Pfu* and (**c**) *Ath* RNase P. All lanes are from the same gel but they have been reordered for better illustration; a thin white line between lanes indicates such reshuffling. F_{C_0} values, indicating the fraction of cleavage at the correct site relative to the total cleavage $[P_{C_0}/(P_{C_0} + P_{M_{+1}})]$ are listed at the bottom of each panel and were obtained by quantitation of the correct and mis-cleaved products. Mean and standard deviation values were calculated from three independent experiments. ND, not detectable. The lane labels are as specified in Figure 3 with Gln indicating the wild-type pre-tRNA^{Gln}. M, the ladder obtained from alkaline hydrolysis of pre-tRNA^{Gln}.

and *Ath* RNase P cleaved with F_{C_0} of ~0.8 and 1, respectively.

We performed various control experiments to verify that the dissimilarity in cleavage-site selection between bacterial and archaeal/eukaryal RNase P was mainly due to their structural/functional variability. First, to eliminate differences in assay conditions as a possible reason for disparities in fidelity of processing (Figure 4), we tested *Eco* RNase P at 55°C and in 30 mM Mg^{2+}, conditions employed for assaying *in vitro* assembled *Pfu* RNase P. At these conditions, the mis-cleavage trend of *Eco* RNase P is largely unchanged compared to assays performed at 37°C and 10 mM Mg^{2+}, which are optimal for *Eco* RNase P (not shown). The reciprocal experiment wherein *Pfu* RNase P is tested under conditions optimal for *Eco* RNase P could not be performed since the *in vitro* reconstituted *Pfu* RNase P shows poor activity at 37°C and 10 mM Mg^{2+}. Second, to ensure that the observations with *Pfu* RNase P are not restricted to type A archaeal RNase P, we examined cleavage of the different pre-tRNA^{Gln} derivatives by *in vitro* reconstituted RNase P from *Mja* (19), a type M RNase P. The cleavage-site selection exhibited by *Mja* RNase P mirrored its *Pfu* counterpart (not shown). Finally, despite the robust biochemical reconstitution of archaeal RNase P, the possibility remained that our observed cleavage-site bias toward C_0 with *in vitro* reconstituted archaeal RNase P (Figure 4) could differ from that of native archaeal RNase P. The availability of partially purified RNase P from *Methanococcus maripaludis* (17) allowed us to dispel this

Downloaded from https://academic.oup.com/nar/article-abstract/40/10/4666/2411132
by guest
on 23 July 2018

concern—this native holoenzyme preparation processed pre-tRNA^{Gln} and its derivatives with $F_{C_0} = 0.8$ to 0.9, consistent with our findings on *Pfu* and *Mja* RNase P assembled *in vitro* using the respective RPR + 4 RPPs (Figure 4; data not shown). Thus, the contribution to fidelity of archaeal RPPs other than RPP21•RPP29 and POP5•RPP30 in the native enzyme (17,85) has to be small given that $F_{C_0} = 0.8$ to 0.9 even in the presence of only these four RPPs.

DISCUSSION

Archaeal RPPs synergistically influence the RPR's cleavage-site selection and rate of processing of pre-tRNA^{Gln}

The synergistic effect of the archaeal RPPs on the cognate RPR's rate and fidelity of processing of pre-tRNA^{Gln} (Figure 2 and Table 2) could be rationalized by the interaction of RPP binary complexes with different parts of the pre-tRNA either directly or through the RPR. Archaeal RPRs, like their bacterial counterparts, can be demarcated into a specificity (S) domain that binds the pre-tRNA's TSL, and a catalytic (C) domain that cleaves the pre-tRNA; moreover, RPP21•RPP29 and POP5•RPP30 footprint on the S and C domains, respectively (19,86). In the context of these specific interactions with the RPR, we contend that cleavage-site selection is influenced by (i) RPP21•RPP29 interacting with the TSL region, and (ii) POP5•RPP30 with sequence/structures near the cleavage site (e.g. the 5′-leader) in the pre-tRNA. Several observations support this idea. First, a recent study examining *Pfu* RPR-mediated cleavages of model substrates, with either an intact T loop or a GAAA tetraloop, revealed that the *Pfu* RPR's S domain could recognize the TSL in these model substrates only in the presence of RPP21•RPP29 (87). Second, given the striking similarity in the tertiary structures of archaeal (and possibly eukaryal) POP5 and bacterial RPP (88,89), and the ability of the bacterial RPP to recognize the 5′-leader of the pre-tRNA (25–27), it is likely that POP5 plays a similar role. Lastly, a gel-shift analysis demonstrated that of the seven recombinant human RPPs tested, only RPP21 and RPP14 (a paralog of POP5) bound pre-tRNA^{Tyr} in a specific manner (90), although the sites of interaction in the pre-tRNA were not mapped.

We stress that inter-domain cooperation in RNase P catalysis is critical for the synergy observed with the two RPP complexes. The ability of RPP21•RPP29 to position an atypical pre-tRNA optimally in the S domain must somehow enable efficient and correct cleavage by the C domain complexed with POP5•RPP30. The distinct functions of the two RPR domains, with or without their associated RPPs, make inter-domain crosstalk obligatory. The recent finding of an S-domain mutation in the TBS of *Eco* RPR that changes the nature and rate of mis-cleavage of a model substrate (by the C domain) reinforces this idea of inter-domain cooperation in cleavage-site selection (91).

The above structural perspective helps inform a kinetic model to understand how archaeal RPPs increase F_{C_0} by their ability to selectively favor the rate of correct cleavage (k_{C_0}) relative to mis-cleavage ($k_{M_{+1}}$). Such preferential increases in k_{C_0} might result either from favorably affecting substrate docking for correct cleavage [by changing K_{C_0}, the equilibrium constant for $E-S \leftrightarrows ES_{C_0}$, or through enhancing the rate of cleavage at C_0 (by changing either K_{conf}, the equilibrium constant for $ES \leftrightarrows ES^*$, or k_c that dictates $ES^* \rightarrow E+P$; the latter is not considered for reasons discussed elsewhere (16,19,70)]. In fact, since binding/docking and cleavage are coupled (Scheme 1), a synergistic increase in the rate of correct cleavage of a non-consensus pre-tRNA would be expected in the presence of both RPP complexes if each RPP pair selectively contributed to K_{C_0} or K_{conf}, a premise supported by previous studies (16,19).

Our earlier single-turnover kinetic studies involving *cis* and *trans* cleavage of a consensus pre-tRNA revealed that while RPP21•RPP29 promotes substrate binding by 16-fold through a decrease in K_S (the dissociation constant for ES formation), POP5•RPP30 increases the archaeal RPR's cleavage rate by ~100-fold probably by enhancing K_{conf} (16,19). In a related vein, we believe that RPP21•RPP29 favorably influences K_{C_0} at the expense of $K_{M_{+1}}$ and thereby increases $k_{C_0}/k_{M_{+1}}$ during self-cleavage of pre-tRNA^{Gln}-*Mja* RPR. The ability of POP5•RPP30 to increase the rate of pre-tRNA^{Gln}-*Mja* RPR cleavage at C_0 (1570-fold) and M_{+1} (450-fold) is presumably due to its promoting ES* formation for both correct cleavage and mis-cleavage ($ES_{C_0} \leftrightarrows ES^*_{C_0}$ and $ES_{M_{+1}} \leftrightarrows ES^*_{M_{+1}}$; Table 2), albeit preferentially for $ES^*_{C_0}$ thus accounting for the increase in $k_{C_0}/k_{M_{+1}}$. Hence, the synergistic increase in the correct cleavage that we observed in the presence of both RPP complexes must reflect their collective ability to favor formation of both ES_{C_0} and $ES^*_{C_0}$, and the cumulative gains from affecting both concomitantly.

POP5•RPP30 normalizes the rate of processing of consensus and non-consensus pre-tRNAs

Our studies uncovered the ability of POP5•RPP30 to increase the archaeal RPR's cleavage rate of the non-consensus pre-tRNA^{Gln} to that observed with pre-tRNA^{Tyr}, a consensus representative. The rate of self-processing of pre-tRNA^{Gln}-*Mja* RPR alone (at C_0) is 286-fold slower than that for pre-tRNA^{Tyr}-*Mja* RPR (Table 2). However, when both RPP complexes are present, the rates of self-processing by these two conjugates differ only by 2.8-fold. This remarkable narrowing of the difference in rates is largely due to the 1570-fold increase in k_{C_0} facilitated by POP5•RPP30 (Table 2). These findings mirror the observation that bacterial RPP normalizes the cognate RPR's rate of cleavage of different pre-tRNAs by altering its energetic contributions to substrate binding and enhancing the rate of RPR-mediated cleavage (25,69,70). To better understand this functional convergent evolution, it would be instructive to compare the mechanisms used by archaeal POP5 and bacterial RPP to equalize the processing rates of different pre-tRNAs by their cognate RPRs.

Downloaded from https://academic.oup.com/nar/article-abstract/40/10/4666/2411132
by guest
on 23 July 2018

Similarities and differences in substrate recognition by RNase P from the three domains of life

All three RNase P variants recognize and cleave pre-tRNA^{Gln} with deleted D or AC stem but not a T stem. Such recognition features noted before for bacterial and eukaryal RNase P (with other pre-tRNAs) can now be extended to archaeal RNase P. The indispensable nature of the TSL for pre-tRNA recognition by RNase P in all three domains of life may be attributable to the coevolution of RNase P and pre-tRNAs. RNase P-mediated 5′-maturation of pre-tRNAs has been suggested to precede 3′-maturation and intron splicing (1,92). Since RNase P processes all pre-tRNAs, some recognition motifs must be universally conserved in all of them. If an intron is present, it is typically located in the anticodon loop of pre-tRNAs (1), occasionally in the D and variable loops, and seldom in the T loop (93). Thus, if RNase P evolved to recognize a largely invariant module in all pre-tRNAs, then the rarely disrupted TSL seems a good choice.

Our results suggest that despite thematic parallels, bacterial RNase P is more reliant on the native tertiary structure of atypical pre-tRNAs such as pre-tRNA^{Gln} for correct cleavage compared to archaeal and eukaryal RNase P. This assertion is borne out by results from previous studies (31,32,43,65) and also by our observation that when the native tertiary structure of pre-tRNA^{Gln} is perturbed (e.g. pre-tRNA^{Gln}D^{+} variants, Figure 3), the mis-cleavage at M_{+1} is enhanced from ~30% to 70% (with F_{C_0} decreasing from 0.7 to 0.3; Figure 4). The ability of protein-rich archaeal and eukaryal RNase P, in contrast to their bacterial cousins, to process pre-tRNA^{Gln} and its mutant derivatives with $F_{C_0} = 0.8$ to 1 reflects their high fidelity even when dealing with non-native pre-tRNA structures and indicates an unexpected tolerance to structural deviations from the pre-tRNA consensus.

Protein-rich RNase P confers more flexibility in substrate-recognition?

In a primordial RNA world setting, if the RPR processed only a few ncRNAs and pre-tRNAs (extant or earlier versions), maintaining a common suite of recognition determinants would not have imposed significant evolutionary constraints. However, sequence drift would have been inevitable given the recombinogenic potential of tRNA-encoding genes (92,94) and the subsequent functional specialization of tRNAs. Thus, strict adherence to the RPR's recognition determinants would have been difficult. It has been suggested that association of the bacterial RPR with an RPP likely provided a countermeasure to alleviate possible recognition/catalytic defects in the RPR caused by sequence variation in pre-tRNAs (25,69,70). Since nucleotide identities at −1 and +1 positions in tRNAs (Table 1) are not as conserved in eukarya as in bacteria, eukaryal RPPs, with unique RNA-binding motifs and a combinatorial capability to fulfill a minimum threshold of contacts, might permit equally efficient binding/cleavage of multiple pre-tRNAs or related RNAs that share few common determinants (not only at N_{-1} and N_{+1}/N_{+72} but elsewhere in the substrate). For example, two human ncRNAs, the 7-kb MALAT1 that is up-regulated in many cancers and the 20-kb Men β involved in the formation of paraspeckles, have a tRNA-like structure, albeit lacking consensus structural elements, and are processed by human RNase P (50,51). Our finding that archaeal and eukaryal RNase P cleave with high fidelity even those substrates that deviate significantly from the pre-tRNA consensus sequence/fold suggests that the multiple archaeal and eukaryal RPPs could promote functional versatility while retaining both speed and accuracy (6,72,95).

With the endonucleolytic activity residing in the RPR, association with multiple RPPs might have facilitated remodeling the archaeal/eukaryal RPR's active site to enable a broader role for protein-rich RNase P in processing and turnover of RNAs that lack tRNA motifs. The ability of yeast RNase P to cleave certain short-lived ncRNAs, mRNAs, and artificial ssRNAs suggests accommodation of a broad range of substrates with little resemblance to pre-tRNAs (52–56). Functional diversification through partial alterations in the subunit composition of an RNP is also exemplified by yeast/human RNase MRP, an RNase P-related endonuclease involved in maturation of rRNAs and turnover of select mRNAs (96–98). RNase MRP contains an RNA subunit that is structurally related to the RPR and up to 10 protein subunits, of which eight are shared with RNase P. A SELEX-based approach revealed that yeast RNase MRP displays broad substrate specificity *in vitro* including cleavage of ssRNAs (99); although this trait is shared with RNase P, the two enzymes use different recognition determinants during cleavage of ssRNAs. These observations collectively support the premise that increased protein content in these related catalytic RNPs might underlie their functional plasticity, echoing the key inference from this study.

SUPPLEMENTARY DATA

Supplementary Data are available at NAR Online: Supplementary Tables 1 and 2.

ACKNOWLEDGEMENTS

The authors are grateful to Drs. Patricia Chan and Todd Lowe (University of California, Santa Cruz) for making changes to the genomic tRNA database that enables users to determine the N_{-1} and N_{+1} variations. The authors thank Professor E. J. Behrman (OSU) for comments on the manuscript.

FUNDING

National Science Foundation grants [MCB 0238233 (CAREER), DBI 0509744 (SGER) and MCB 0843543 to V.G.]; and a National Institutes of Health Grant (GM067807 to M.P.F. and V.G.). Funding for open access charge: National Science Foundation.

Conflict of interest statement. None declared.

Downloaded from https://academic.oup.com/nar/article-abstract/40/10/4666/2411132
by guest
on 23 July 2018

REFERENCES

1. Phizicky,E.M. and Hopper,A.K. (2010) tRNA biology charges to the front. *Genes Dev.*, **24**, 1832–1860.
2. Gobert,A., Gutmann,B., Taschner,A., Gossringer,M., Holzmann,J., Hartmann,R.K., Rossmanith,W. and Giege,P. (2010) A single Arabidopsis organellar protein has RNase P activity. *Nat. Struct. Mol. Biol.*, **17**, 740–744.
3. Holzmann,J., Frank,P., Loffler,E., Bennett,K.L., Gerner,C. and Rossmanith,W. (2008) RNase P without RNA: identification and functional reconstitution of the human mitochondrial tRNA processing enzyme. *Cell*, **135**, 462–474.
4. Esakova,O. and Krasilnikov,A.S. (2010) Of proteins and RNA: the RNase P/MRP family. *RNA*, **16**, 1725–1747.
5. Evans,D., Marquez,S.M. and Pace,N.R. (2006) RNase P: interface of the RNA and protein worlds. *Trends Biochem. Sci.*, **31**, 333–341.
6. Jarrous,N. and Gopalan,V. (2010) Archaeal/eukaryal RNase P: subunits, functions and RNA diversification. *Nucleic Acids Res.*, **38**, 7885–7894.
7. Lai,L.B., Vioque,A., Kirsebom,L.A. and Gopalan,V. (2010) Unexpected diversity of RNase P, an ancient tRNA processing enzyme: challenges and prospects. *FEBS Lett.*, **584**, 287–296.
8. Walker,S.C. and Engelke,D.R. (2006) Ribonuclease P: the evolution of an ancient RNA enzyme. *Crit. Rev. Biochem. Mol. Biol.*, **41**, 77–102.
9. McClain,W.H., Lai,L.B. and Gopalan,V. (2010) Trials, travails and triumphs: An account of RNA catalysis in RNase P. *J. Mol. Biol.*, **397**, 627–646.
10. Guerrier-Takada,C., Gardiner,K., Marsh,T., Pace,N. and Altman,S. (1983) The RNA moiety of ribonuclease P is the catalytic subunit of the enzyme. *Cell*, **35**, 849–857.
11. Kikovska,E., Svard,S.G. and Kirsebom,L.A. (2007) Eukaryotic RNase P RNA mediates cleavage in the absence of protein. *Proc. Natl Acad. Sci. USA*, **104**, 2062–2067.
12. Pannucci,J.A., Haas,E.S., Hall,T.A., Harris,J.K. and Brown,J.W. (1999) RNase P RNAs from some Archaea are catalytically active. *Proc. Natl Acad. Sci. USA*, **96**, 7803–7808.
13. Chamberlain,J.R., Lee,Y., Lane,W.S. and Engelke,D.R. (1998) Purification and characterization of the nuclear RNase P holoenzyme complex reveals extensive subunit overlap with RNase MRP. *Genes Dev.*, **12**, 1678–1690.
14. Ozeki,H., Sakano,H., Yamada,S., Ikemura,T. and Shimura,Y. (1975) Temperature-sensitive mutants of Escherichia coli defective in tRNA biosynthesis. *Brookhaven Symp. Biol.*, 89–105.
15. Schedl,P. and Primakoff,P. (1973) Mutants of Escherichia coli thermosensitive for the synthesis of transfer RNA. *Proc. Natl Acad. Sci. USA*, **70**, 2091–2095.
16. Chen,W.Y., Pulukkunat,D.K., Cho,I.M., Tsai,H.Y. and Gopalan,V. (2010) Dissecting functional cooperation among protein subunits in archaeal RNase P, a catalytic ribonucleoprotein complex. *Nucleic Acids Res.*, **38**, 8316–8327.
17. Cho,I.M., Lai,L.B., Susanti,D., Mukhopadhyay,B. and Gopalan,V. (2010) Ribosomal protein L7Ae is a subunit of archaeal RNase P. *Proc. Natl Acad. Sci. USA*, **107**, 14573–14578.
18. Hall,T.A. and Brown,J.W. (2002) Archaeal RNase P has multiple protein subunits homologous to eukaryotic nuclear RNase P proteins. *RNA*, **8**, 296–306.
19. Pulukkunat,D.K. and Gopalan,V. (2008) Studies on Methanocaldococcus jannaschii RNase P reveal insights into the roles of RNA and protein cofactors in RNase P catalysis. *Nucleic Acids Res.*, **36**, 4172–4180.
20. Tsai,H.Y., Pulukkunat,D.K., Woznick,W.K. and Gopalan,V. (2006) Functional reconstitution and characterization of Pyrococcus furiosus RNase P. *Proc. Natl Acad. Sci. USA*, **103**, 16147–16152.
21. Li,D., Willkomm,D.K. and Hartmann,R.K. (2009) Minor changes largely restore catalytic activity of archaeal RNase P RNA from Methanothermobacter thermoautotrophicus. *Nucleic Acids Res.*, **37**, 231–242.
22. Christian,E.L., Zahler,N.H., Kaye,N.M. and Harris,M.E. (2002) Analysis of substrate recognition by the ribonucleoprotein endonuclease RNase P. *Methods*, **28**, 307–322.
23. Kirsebom,L.A. and Trobro,S. (2009) RNase P RNA-mediated cleavage. *IUBMB Life*, **61**, 189–200.
24. Crary,S.M., Niranjanakumari,S. and Fierke,C.A. (1998) The protein component of Bacillus subtilis ribonuclease P increases catalytic efficiency by enhancing interactions with the 5′ leader sequence of pre-tRNAAsp. *Biochemistry*, **37**, 9409–9416.
25. Koutmou,K.S., Zahler,N.H., Kurz,J.C., Campbell,F.E., Harris,M.E. and Fierke,C.A. (2010) Protein-precursor tRNA contact leads to sequence-specific recognition of 5′ leaders by bacterial ribonuclease P. *J. Mol. Biol.*, **396**, 195–208.
26. Niranjanakumari,S., Stams,T., Crary,S.M., Christianson,D.W. and Fierke,C.A. (1998) Protein component of the ribozyme ribonuclease P alters substrate recognition by directly contacting precursor tRNA. *Proc. Natl Acad. Sci. USA*, **95**, 15212–15217.
27. Rueda,D., Hsieh,J., Day-Storms,J.J., Fierke,C.A. and Walter,N.G. (2005) The 5′ leader of precursor tRNAAsp bound to the *Bacillus subtilis* RNase P holoenzyme has an extended conformation. *Biochemistry*, **44**, 16130–16139.
28. Tsai,H.Y., Masquida,B., Biswas,R., Westhof,E. and Gopalan,V. (2003) Molecular modeling of the three-dimensional structure of the bacterial RNase P holoenzyme. *J. Mol. Biol.*, **325**, 661–675.
29. Brannvall,M., Fredrik Pettersson,B.M. and Kirsebom,L.A. (2002) The residue immediately upstream of the RNase P cleavage site is a positive determinant. *Biochimie*, **84**, 693–703.
30. Zahler,N.H., Christian,E.L. and Harris,M.E. (2003) Recognition of the 5′ leader of pre-tRNA substrates by the active site of ribonuclease P. *RNA*, **9**, 734–745.
31. Zahler,N.H., Sun,L., Christian,E.L. and Harris,M.E. (2005) The pre-tRNA nucleotide base and 2′-hydroxyl at N(-1) contribute to fidelity in tRNA processing by RNase P. *J. Mol. Biol.*, **345**, 969–985.
32. Brannvall,M., Kikovska,E., Wu,S. and Kirsebom,L.A. (2007) Evidence for induced fit in bacterial RNase P RNA-mediated cleavage. *J. Mol. Biol.*, **372**, 1149–1164.
33. Loria,A. and Pan,T. (1997) Recognition of the T stem-loop of a pre-tRNA substrate by the ribozyme from Bacillus subtilis ribonuclease P. *Biochemistry*, **36**, 6317–6325.
34. Pan,T., Loria,A. and Zhong,K. (1995) Probing of tertiary interactions in RNA: 2′-hydroxyl-base contacts between the RNase P RNA and pre-tRNA. *Proc. Natl Acad. Sci. USA*, **92**, 12510–12514.
35. Kirsebom,L.A. and Svard,S.G. (1994) Base pairing between *Escherichia coli* RNase P RNA and its substrate. *EMBO J.*, **13**, 4870–4876.
36. Reiter,N.J., Osterman,A., Torres-Larios,A., Swinger,K.K., Pan,T. and Mondragon,A. (2010) Structure of a bacterial ribonuclease P holoenzyme in complex with tRNA. *Nature*, **468**, 784–789.
37. Hardt,W.D., Schlegl,J., Erdmann,V.A. and Hartmann,R.K. (1993) Role of the D arm and the anticodon arm in tRNA recognition by eubacterial and eukaryotic RNase P enzymes. *Biochemistry*, **32**, 13046–13053.
38. Yuan,Y. and Altman,S. (1995) Substrate recognition by human RNase P: identification of small, model substrates for the enzyme. *EMBO J.*, **14**, 159–168.
39. Carrara,G., Calandra,P., Fruscoloni,P. and Tocchini-Valentini,G.P. (1995) Two helices plus a linker: a small model substrate for eukaryotic RNase P. *Proc. Natl Acad. Sci. USA*, **92**, 2627–2631.
40. McClain,W.H., Guerrier-Takada,C. and Altman,S. (1987) Model substrates for an RNA enzyme. *Science*, **238**, 527–530.
41. Burkard,U., Willis,I. and Soll,D. (1988) Processing of histidine transfer RNA precursors. Abnormal cleavage site for RNase P. *J. Biol. Chem.*, **263**, 2447–2451.
42. Holm,P.S. and Krupp,G. (1992) The acceptor stem in pre-tRNAs determines the cleavage specificity of RNase P. *Nucleic Acids Res.*, **20**, 421–423.
43. Krupp,G., Kahle,D., Vogt,T. and Char,S. (1991) Sequence changes in both flanking sequences of a pre-tRNA influence the cleavage specificity of RNase P. *J. Mol. Biol.*, **217**, 637–648.
44. Alifano,P., Rivellini,F., Piscitelli,C., Arraiano,C.M., Bruni,C.B. and Carlomagno,M.S. (1994) Ribonuclease E provides substrates for ribonuclease P-dependent processing of a polycistronic mRNA. *Genes Dev.*, **8**, 3021–3031.

Downloaded from https://academic.oup.com/nar/article-abstract/40/10/4666/2411132
by guest
on 23 July 2018

45. Bothwell,A.L., Garber,R.L. and Altman,S. (1976) Nucleotide sequence and in vitro processing of a precursor molecule to *Escherichia coli* 4.5 S RNA. *J. Biol. Chem.*, **251**, 7709–7716.
46. Hartmann,R.K., Heinrich,J., Schlegl,J. and Schuster,H. (1995) Precursor of C4 antisense RNA of bacteriophages P1 and P7 is a substrate for RNase P of Escherichia coli. *Proc. Natl Acad. Sci. USA*, **92**, 5822–5826.
47. Komine,Y., Kitabatake,M., Yokogawa,T., Nishikawa,K. and Inokuchi,H. (1994) A tRNA-like structure is present in 10Sa RNA, a small stable RNA from Escherichia coli. *Proc. Natl Acad. Sci. USA*, **91**, 9223–9227.
48. Li,Y. and Altman,S. (2004) Polarity effects in the lactose operon of Escherichia coli. *J. Mol. Biol.*, **339**, 31–39.
49. Mans,R.M., Guerrier-Takada,C., Altman,S. and Pleij,C.W. (1990) Interaction of RNase P from Escherichia coli with pseudoknotted structures in viral RNAs. *Nucleic Acids Res.*, **18**, 3479–3487.
50. Sunwoo,H., Dinger,M.E., Wilusz,J.E., Amaral,P.P., Mattick,J.S. and Spector,D.L. (2009) MEN epsilon/beta nuclear-retained non-coding RNAs are up-regulated upon muscle differentiation and are essential components of paraspeckles. *Genome Res.*, **19**, 347–359.
51. Wilusz,J.E., Freier,S.M. and Spector,D.L. (2008) 3′ end processing of a long nuclear-retained noncoding RNA yields a tRNA-like cytoplasmic RNA. *Cell*, **135**, 919–932.
52. Coughlin,D.J., Pleiss,J.A., Walker,S.C., Whitworth,G.B. and Engelke,D.R. (2008) Genome-wide search for yeast RNase P substrates reveals role in maturation of intron-encoded box C/D small nucleolar RNAs. *Proc. Natl Acad. Sci. USA*, **105**, 12218–12223.
53. Marvin,M.C., Clauder-Munster,S., Walker,S.C., Sarkeshik,A., Yates,J.R. 3rd, Steinmetz,L.M. and Engelke,D.R. (2011) Accumulation of noncoding RNA due to an RNase P defect in Saccharomyces cerevisiae. *RNA*, **17**, 1441–1450.
54. Marvin,M.C., Walker,S.C., Fierke,C.A. and Engelke,D.R. (2011) Binding and cleavage of unstructured RNA by nuclear RNase P. *RNA*, **17**, 1429–1440.
55. Samanta,M.P., Tongprasit,W., Sethi,H., Chin,C.S. and Stolc,V. (2006) Global identification of noncoding RNAs in Saccharomyces cerevisiae by modulating an essential RNA processing pathway. *Proc. Natl Acad. Sci. USA*, **103**, 4192–4197.
56. Yang,L. and Altman,S. (2007) A noncoding RNA in Saccharomyces cerevisiae is an RNase P substrate. *RNA*, **13**, 682–690.
57. Pascual,A. and Vioque,A. (1999) Substrate binding and catalysis by ribonuclease P from cyanobacteria and Escherichia coli are affected differently by the 3′ terminal CCA in tRNA precursors. *Proc. Natl Acad. Sci. USA*, **96**, 6672–6677.
58. Tsai,H.Y., Lai,L.B. and Gopalan,V. (2002) A modified pBluescript-based vector for facile cloning and transcription of RNAs. *Anal. Biochem.*, **303**, 214–217.
59. Vioque,A., Arnez,J. and Altman,S. (1988) Protein-RNA interactions in the RNase P holoenzyme from Escherichia coli. *J. Mol. Biol.*, **202**, 835–848.
60. Gopalan,V., Baxevanis,A.D., Landsman,D. and Altman,S. (1997) Analysis of the functional role of conserved residues in the protein subunit of ribonuclease P from Escherichia coli. *J. Mol. Biol.*, **267**, 818–829.
61. Chen,W.Y., Xu,Y., Cho,I.M., Oruganti,S.V., Foster,M.P. and Gopalan,V. (2011) Cooperative RNP assembly: complementary rescue of structural defects by protein and RNA subunits of archaeal RNase P. *J. Mol. Biol.*, **411**, 368–383.
62. Chan,P.P. and Lowe,T.M. (2009) GtRNAdb: a database of transfer RNA genes detected in genomic sequence. *Nucleic Acids Res.*, **37**, D93–D97.
63. Sprinzl,M., Horn,C., Brown,M., Ioudovitch,A. and Steinberg,S. (1998) Compilation of tRNA sequences and sequences of tRNA genes. *Nucleic Acids Res.*, **26**, 148–153.
64. Kikovska,E., Brannvall,M. and Kirsebom,L.A. (2006) The exocyclic amine at the RNase P cleavage site contributes to substrate binding and catalysis. *J. Mol. Biol.*, **359**, 572–584.
65. Kikovska,E., Brannvall,M., Kufel,J. and Kirsebom,L.A. (2005) Substrate discrimination in RNase P RNA-mediated cleavage: importance of the structural environment of the RNase P cleavage site. *Nucleic Acids Res.*, **33**, 2012–2021.
66. Kirsebom,L.A. and Svard,S.G. (1992) The kinetics and specificity of cleavage by RNase P is mainly dependent on the structure of the amino acid acceptor stem. *Nucleic Acids Res.*, **20**, 425–432.
67. Svard,S.G. and Kirsebom,L.A. (1992) Several regions of a tRNA precursor determine the Escherichia coli RNase P cleavage site. *J. Mol. Biol.*, **227**, 1019–1031.
68. Loria,A. and Pan,T. (1998) Recognition of the 5′ leader and the acceptor stem of a pre-tRNA substrate by the ribozyme from Bacillus subtilis RNase P. *Biochemistry*, **37**, 10126–10133.
69. Sun,L., Campbell,F.E., Yandek,L.E. and Harris,M.E. (2010) Binding of C5 protein to P RNA enhances the rate constant for catalysis for P RNA processing of pre-tRNAs lacking a consensus (+ 1)/C(+ 72) pair. *J. Mol. Biol.*, **395**, 1019–1037.
70. Sun,L., Campbell,F.E., Zahler,N.H. and Harris,M.E. (2006) Evidence that substrate-specific effects of C5 protein lead to uniformity in binding and catalysis by RNase P. *EMBO J.*, **25**, 3998–4007.
71. Sun,L. and Harris,M.E. (2007) Evidence that binding of C5 protein to P RNA enhances ribozyme catalysis by influencing active site metal ion affinity. *RNA*, **13**, 1505–1515.
72. Gopalan,V. (2007) Uniformity amid diversity in RNase P. *Proc. Natl Acad. Sci. USA*, **104**, 2031–2032.
73. Harris,J.K., Haas,E.S., Williams,D., Frank,D.N. and Brown,J.W. (2001) New insight into RNase P RNA structure from comparative analysis of the archaeal RNA. *RNA*, **7**, 220–232.
74. Hsieh,J. and Fierke,C.A. (2009) Conformational change in the Bacillus subtilis RNase P holoenzyme–pre-tRNA complex enhances substrate affinity and limits cleavage rate. *RNA*, **15**, 1565–1577.
75. Hsieh,J., Koutmou,K.S., Rueda,D., Koutmos,M., Walter,N.G. and Fierke,C.A. (2010) A divalent cation stabilizes the active conformation of the B. subtilis RNase P x pre-tRNA complex: a role for an inner-sphere metal ion in RNase P. *J. Mol. Biol.*, **400**, 38–51.
76. Koutmou,K.S., Hsieh,J. and Fierke,C.A. (2009) In: Liu,F.A.S. (ed.), *Ribonuclease P*. Springer Verlag, New York, pp. 93–112.
77. Pomeranz Krummel,D.A. and Altman,S. (1999) Multiple binding modes of substrate to the catalytic RNA subunit of RNase P from Escherichia coli. *RNA*, **5**, 1021–1033.
78. Rosenblad,M.A., Lopez,M.D., Piccinelli,P. and Samuelsson,T. (2006) Inventory and analysis of the protein subunits of the ribonucleases P and MRP provides further evidence of homology between the yeast and human enzymes. *Nucleic Acids Res.*, **34**, 5145–5156.
79. Franklin,S.E., Zwick,M.G. and Johnson,J.D. (1995) Characterization and partial purification of two pre-tRNA 5′-processing activities from Daucus carrota (carrot) suspension cells. *Plant J.*, **7**, 553–563.
80. Pulukkunat,D.K. (2002) M.S. Thesis. The Ohio State University, Columbus, OH.
81. Reckard,J.F. 3rd (2000) M.S. Thesis. The Ohio State University, Columbus, OH.
82. Lai,L.B., Bernal-Bayard,P., Mohannath,G., Lai,S.M., Gopalan,V. and Vioque,A. (2011) A functional RNase P protein subunit of bacterial origin in some eukaryotes. *Mol. Genet. Genomics*, **286**, 359–369.
83. Ioudovitch,A. and Steinberg,S.V. (1999) Structural compensation in an archaeal selenocysteine transfer RNA. *J. Mol. Biol.*, **290**, 365–371.
84. Kahle,D., Wehmeyer,U. and Krupp,G. (1990) Substrate recognition by RNase P and by the catalytic M1 RNA: identification of possible contact points in pre-tRNAs. *EMBO J.*, **9**, 1929–1937.
85. Fukuhara,H., Kifusa,M., Watanabe,M., Terada,A., Honda,T., Numata,T., Kakuta,Y. and Kimura,M. (2006) A fifth protein subunit Ph1496p elevates the optimum temperature for the ribonuclease P activity from Pyrococcus horikoshii OT3. *Biochem. Biophys. Res. Commun.*, **343**, 956–964.
86. Xu,Y., Amero,C.D., Pulukkunat,D.K., Gopalan,V. and Foster,M.P. (2009) Solution structure of an archaeal RNase P binary protein complex: formation of the 30-kDa complex between Pyrococcus furiosus RPP21 and RPP29 is accompanied

Downloaded from https://academic.oup.com/nar/article-abstract/40/10/4666/2411132
by guest
on 23 July 2018

by coupled protein folding and highlights critical features for protein-protein and protein-RNA interactions. *J. Mol. Biol.*, **393**, 1043–1055.
87. Sinapah,S., Wu,S., Chen,Y., Pettersson,B.M., Gopalan,V. and Kirsebom,L.A. (2011) Cleavage of model substrates by archaeal RNase P: role of protein cofactors in cleavage-site selection. *Nucleic Acids Res.*, **39**, 1105–1116.
88. Kawano,S., Nakashima,T., Kakuta,Y., Tanaka,I. and Kimura,M. (2006) Crystal structure of protein Ph1481p in complex with protein Ph1877p of archaeal RNase P from Pyrococcus horikoshii OT3: implication of dimer formation of the holoenzyme. *J. Mol. Biol.*, **357**, 583–591.
89. Wilson,R.C., Bohlen,C.J., Foster,M.P. and Bell,C.E. (2006) Structure of Pfu Pop5, an archaeal RNase P protein. *Proc. Natl Acad. Sci. USA*, **103**, 873–878.
90. Jarrous,N., Reiner,R., Wesolowski,D., Mann,H., Guerrier-Takada,C. and Altman,S. (2001) Function and subnuclear distribution of Rpp21, a protein subunit of the human ribonucleoprotein ribonuclease P. *RNA*, **7**, 1153–1164.
91. Wu,S., Chen,Y., Lindell,M., Mao,G. and Kirsebom,L.A. (2011) Functional coupling between a distal interaction and the cleavage site in bacterial RNase P RNA-mediated cleavage. *J. Mol. Biol.*, **411**, 384–396.
92. Hartmann,R.K., Gossringer,M., Spath,B., Fischer,S. and Marchfelder,A. (2009) The making of tRNAs and more - RNase P and tRNase Z. *Prog. Mol. Biol. Transl. Sci.*, **85**, 319–368.
93. Marck,C. and Grosjean,H. (2003) Identification of BHB splicing motifs in intron-containing tRNAs from 18 archaea: evolutionary implications. *RNA*, **9**, 1516–1531.
94. She,Q., Shen,B. and Chen,L. (2004) Archaeal integrases and mechanisms of gene capture. *Biochem. Soc. Trans.*, **32**, 222–226.
95. Marvin,M.C. and Engelke,D.R. (2009) RNase P: increased versatility through protein complexity? *RNA Biol.*, **6**, 40–42.
96. Chu,S., Archer,R.H., Zengel,J.M. and Lindahl,L. (1994) The RNA of RNase MRP is required for normal processing of ribosomal RNA. *Proc. Natl Acad. Sci. USA*, **91**, 659–663.
97. Gill,T., Cai,T., Aulds,J., Wierzbicki,S. and Schmitt,M.E. (2004) RNase MRP cleaves the CLB2 mRNA to promote cell cycle progression: novel method of mRNA degradation. *Mol. Cell. Biol.*, **24**, 945–953.
98. Schmitt,M.E. and Clayton,D.A. (1993) Nuclear RNase MRP is required for correct processing of pre-5.8S rRNA in Saccharomyces cerevisiae. *Mol. Cell. Biol.*, **13**, 7935–7941.
99. Esakova,O., Perederina,A., Quan,C., Berezin,I. and Krasilnikov,A.S. (2011) Substrate recognition by ribonucleoprotein ribonuclease MRP. *RNA*, **17**, 356–364.
100. Brown,J.W. (1999) The ribonuclease P database. *Nucleic Acids Res.*, **27**, 314.

Downloaded from https://academic.oup.com/nar/article-abstract/40/10/4666/2411132
by guest
on 23 July 2018